Reprinted from:

NUCLEAR PHYSICS, VOLUME A105 (1967) No. 2

H. J. ERRAMUSPE

Synchrocyclotron Laboratory, Comisión Nacional de Energía Atómica, Buenos Aires, Argentina

ISOSPIN DEPENDENCE OF THE NUCLEAR OPTICAL POTENTIAL

NORTH-HOLLAND PUBLISHING COMPANY - AMSTERDAM

1.E.7:
2.E

Nuclear Physics **A105** (1967) 569—589;

ISOSPIN DEPENDENCE OF THE NUCLEAR OPTICAL POTENTIAL

H. J. ERRAMUSPE
Synchrocyclotron Laboratory, Comisión Nacional de Energía Atómica, Buenos Aires, Argentina †

Received 20 March 1967

Abstract: The isospin-dependent term in the optical-model potential has been investigated by comparing results obtained from simultaneous fitting of neutron and proton elastic scattering data from ^{59}Co and ^{209}Bi at an energy approximately equal to 14.4 MeV. The coefficient of the nuclear symmetry parameter term is equal to 23.8 ± 3 MeV if the fits were obtained by keeping fixed the imaginary part of the potential. If this part is allowed to vary and only the best fits are taken into consideration $C = 22.8 \pm 4$ MeV.

E NUCLEAR REACTIONS ^{59}Co, ^{209}Bi(p, p), $E = 14.4$ MeV; measured $\sigma(\theta)$; deduced optical potential, isospin term coefficient.

1. Introduction

The proton potential anomaly, which gives rise to a difference between the proton-nucleus and the neutron-nucleus potentials is very well known and has been extensively studied [1-17]).

The dependence of the real nuclear potential depth V on the nuclear symmetry parameter $(N-Z)/A$ was suggested by Green and Sood [15]) and by Lane [18]). Green and Sood studied intensively the different reasons which could give rise to such an anomaly, including the presence of Heisenberg forces, the effect of the exclusion principle, the spin dependence of the nuclear forces, etc.

Lane [19-20]) has pointed out that the nuclear optical potential depends on the isospin and that if a calculation of V is taken as a sum of two-body forces with Heisenberg components and averaged over a Fermi gas, the following expression is obtained:

$$V = u_0 + A^{-1}(\boldsymbol{t} \cdot \boldsymbol{T})v_1 ,$$

where u_0 and v_1 are independent of isospin, N or Z, but depend in general on position and momentum, and $\boldsymbol{t}$ and $\boldsymbol{T}$ are the isospins of the incident nucleon and target nucleus of mass A, respectively.

By averaging this expression with weights proportional to the square of the corresponding Clebsch-Gordan coefficients, the neutron and proton potentials turn out

† Work supported in part by the U.S Atomic Energy Commission.

to be

$$U_n = u_0 + \tfrac{1}{4}\alpha v_1 , \tag{1}$$

$$U_p = u_0 - \tfrac{1}{4}\alpha v_1 - V_c , \tag{2}$$

where $\alpha = (N-Z)/A$ is the nuclear symmetry parameter and V_c a corrective term that takes into account the variation of the kinetic energy of the proton due to the Coulomb barrier (energy dependence of U), which is [21]) approximately equal to $0.4\, Z/A^{\frac{1}{3}}$ MeV. The quantities U and V have negative and positive values, respectively. The formulae can be written in the usual way when $C = \frac{1}{4}v_1$.

As has been pointed out by Lane and later by Hodgson [22]), knowledge of C is important for several distinct classes of phenomena, including nuclear symmetry energies, nuclear scattering data and quasi-elastic scattering to the isospin analogue state of the target nucleus. Moreover, the knowledge of the nuclear symmetry parameter has a special importance in the case of DWBA calculations for direct interactions of the pick-up or stripping type, when the final nucleus is unstable and the optical-model wave functions cannot be obtained via scattering experiments. Data on the nearby nuclei can be made available and through the nuclear symmetry parameter it is possible to find the necessary information.

Since the former methods generally used an indirect approach to evaluate the isospin-dependent term of the nuclear optical potential, it was the purpose of this experiment to find this term in a direct way. Doing this, the intention was to measure the proton elastic differential cross sections on some nuclei, to obtain the neutron data from the literature corresponding to the same nuclei at the same energy (14.4 MeV), by taking advantage of the density of experimental neutron data at this energy, and, finally, try to fit both neutron and proton data at the same time. From the necessary potential differences for the data fitting it would be possible to extract the desired information. Although the inaccuracy of the neutron data was an unfavourable factor, the additional knowledge of the total and non-elastic cross sections for neutrons might be a favourable factor to remove uncertainties.

The nuclei ^{59}Co and ^{209}Bi were selected for study due to the reasons given below.

2. Experimental methods

2.1. EXPERIMENTAL FACILITIES

The experiments were performed using the external 14.4 MeV proton beam of the Columbia University Pupin 91 cm cyclotron. The external beam was directed and focussed in the usual way by using quadrupole lenses, steering magnets, a bending magnet, collimators, etc. as illustrated in fig. 1. Additional quartz in the collimators allowed a visual method for centring the beam. Collimators of different diameters were interchangeable to obtain a good beam geometry.

A scattering chamber especially designed for use with solid-state detectors was mounted and used for long periods of time with an excellent performance [23]).

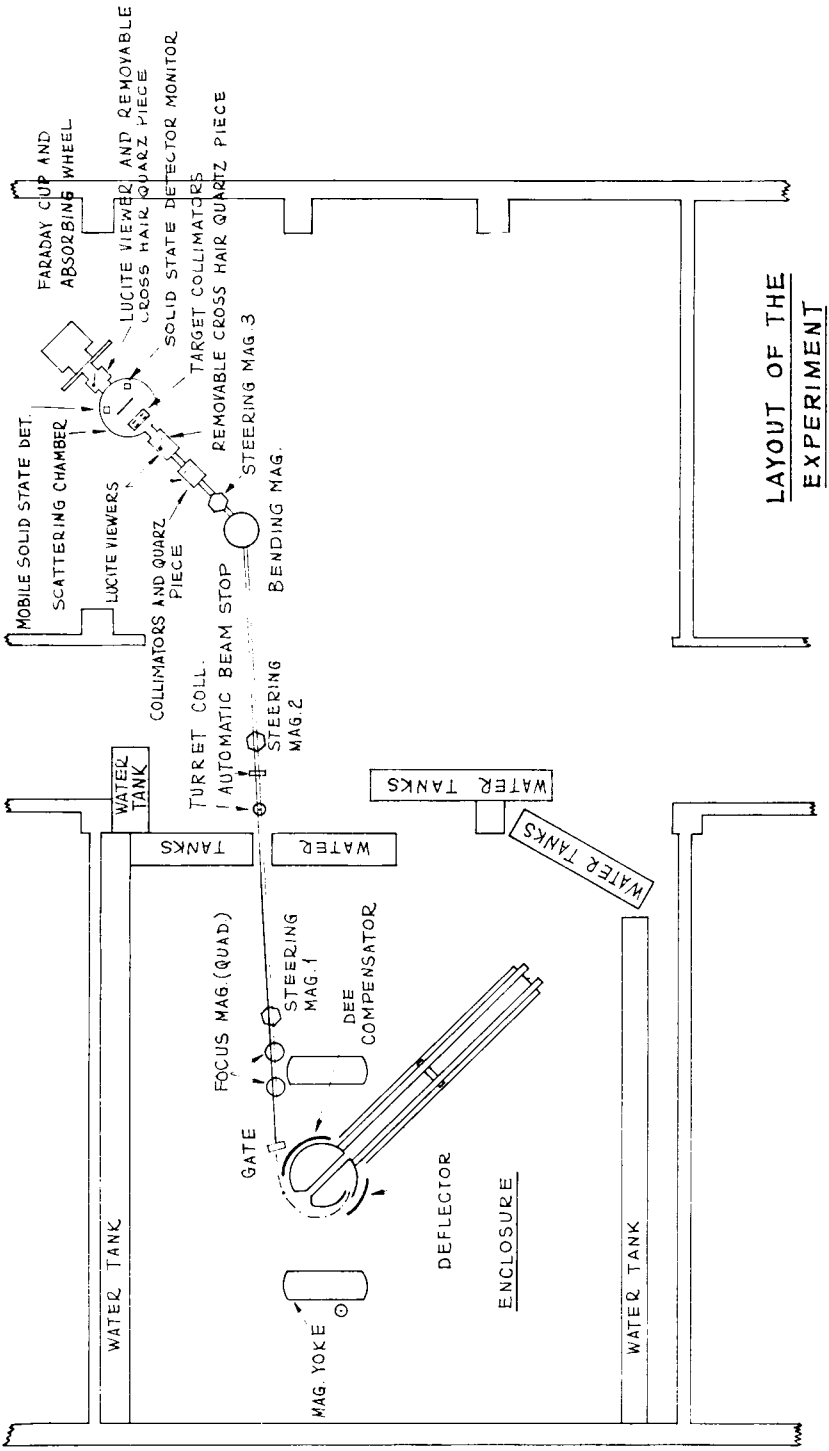

Fig. 1. Layout of the external beam facilities of Columbia University Pupin 91 cm cyclotron.

The beam was collected in a Faraday cup with magnetic suppression of secondary electrons and integrated for data normalization. The energy was measured in the standard way by using aluminium absorbers of variable thicknesses. The good geometry obtained was reflected in the shape of the beam spot on the target, an ellipse of 4×5 mm. The general values of the beam intensity were 3 to 4 nA and, exceptionally, 6 to 8 nA. To keep the pipe at an adequate vacuum, two pumping stations were available, one immediately after the exit of the accelerator room and the other at the end of the system at the Faraday cup.

2.2. EXPERIMENTAL PROCEDURE

The particle detection was made with Si (Li-drifted) solid-state detectors, thick enough to stop the most energetics protons. First, the guard ring system was used [24]) but was finally abandoned because no measurable improving effects were detected. Although good results were obtained with the spring contact method for the detectors, it became a little troublesome and was changed to a new method. Taking advantage of the low neutron background in the experimental area, a new system was developed. A little lucite box with a circular aperture with the side cut at 45° and mirror polished was made. At the other side of the hole the diode was mounted. The front contact was made by dripping a metal point on the side and depositing a thick gold layer on the entire surface, before the diode was mounted. A new thin gold film was deposited after the diode mounting. The contact proved to be excellent for extended periods of time. The connectors were carried through the insulator material of the detector housing.

Interchangeable collimators were used allowing solid angles ranging from 10^{-4} to 8×10^{-6}. The usual value was 1.267×10^{-4} with a semiangle at the centre of 22′. Therefore, no correction was necessary due to finite aperture. Due to the experimental set-up, a wide range of angles from 3° to 170° was possible. Since these small angles were obtained to avoid that too many of the large number of scattered particles at forward angles entered the detector after multiple scattering processes, a 3.5 cm long tube, with a piece of copper at its entrance, was used as a collimator. Copper seems to be one of the best materials to minimize slit scattering effects [25]). The whole design was made so that no multiple scattering processes inside the tube could take place from particles coming from any part of the target. Overlap of measurements corresponding to at least three angles taken with the normal collimators was used as a check of the system.

To avoid detector damage owing to ion bombardment, a high voltage ion protector was installed [26]). Under these conditions, resolutions of the order of 1 % were obtained. In short runs with smaller possibilities of beam energy fluctuations, resolutions of the order of 80 keV for protons of 14.3 MeV were obtained (0.56 %). In long runs (some hours) 130 to 140 keV were usual values.

The energy spread of the beam after collimation was measured. An approximately value of 60 keV was obtained. The detector response was calibrated against energy. An excellent linearity was found from 3.5 MeV to 14.3 MeV.

The integrator calibration was carried out with the known, current, intensity-time method by using a thermostatized high precision resistor and differential voltmeters with 0.01 V maximum sensitivity. The calibrations were made for different simulated beam intensities at the beginning, during and at the end of the data taking period.

The system was aligned optically and by using quartz with cross hairs for centering the beam. A further check was made by using a kinematic method. Proton peaks from the reactions H(p, p)H and ^{12}C(p, p')^{12}C* resulting from the proton bombardment of a polyethylene target, cut across each other at a lab angle of approximately 35° 16′ and are 55° keV apart 0.23° to either side. With detectors of resolution between 80 and 100 keV, it was possible to estimate the maximum absolute angular error to 0.2°.

The formvar backing of the ^{209}Bi target gives rise to carbon and oxygen impurity problems. Nonetheless, the separation of the elastic scattered proton peaks at backward angles due to kinematic differences for different masses, made possible the evaluation of the carbon and oxygen thicknesses with the previous knowledge of their differential cross sections at this energy [27]). We obtained 34 ± 2 μg/cm^2 and 24 ± 2 μg/cm^2 for carbon and oxygen, respectively. The superposition with the ^{209}Bi peak took place for angles smaller than 50°. In all cases the corrections amounted to less than 1.2 %.

Two multi-channel analysers (a RIDL 400-channel, mod. 34-12B and a 256-channel, Argonne type) were used in parallel, one had a bias circuit and threshold different from zero to store useful information only, to minimize the processing data deadtime and the other used in the normal way for kinematic studies.

Hybrid charge sensitive preamplifiers showed a very good performance over extended periods of time and were made by the Columbia University Electronics Laboratory [28]). The integration and differentiation constants were equal (1 μsec), for maximum signal-to-noise ratio [29]). Linearity was better than 0.1 %.

Since absolute differential cross sections were to be measured a verification of the total charge collection was essential.

After traversing the scattering chamber, the unscattered beam is collected in the Faraday cup. Its position was selected so that the solid angle it subtends at the target is sufficiently large that none of the beam multiply scattered in the target is lost. Such was the case for all the elements used in different studies [31]) with the exception of ^{209}Bi.

Theoretically the study was made through the mean square angle corresponding to multiple scattering

$$\theta^2 = \frac{2\pi r_0^2 Z^2 N^2}{\frac{E}{m_0 c^2}} \ln (181 Z^{-\frac{1}{3}}) \Delta x,$$

where the classical radius of the electron $r_0 = e^2/m_0 c^2 = 2.818$ fm, Z is the target

atomic number, N the atoms per cm^3, E the energy of the incident particle, the rest mass of the electron $m_0c^2 = 0.511$ MeV and Δx the target thickness in cm.

The diameter corresponding to this angle was ten times smaller than the minimum diameter of the entrance pipe to the Faraday cup in the ^{59}Co case, as was the situation for the other elements under study [31]). This result practically assures total charge collection. For ^{209}Bi, on the contrary, the situation was more critical.

To corroborate the calculations, an experimental verification was carried out [33]). A thin Al target (0.2 mg/cm^2) was mounted at the entrance of the scattering chamber together with a solid state detector placed inside the chamber, at a forward angle facing this auxiliary target at a distance a little smaller than the radius of the scattering chamber and protected by a baffle to avoid being reached by backscattered particles from the main target. Counts of the order of 10^5 were taken under the elastic peak for target-out and target-in positions of the main target. Any loss of particles scattered in the latter would be revealed by this method. The agreement was within the statistical error for ^{59}Co as expected. For ^{209}Bi, a loss of 3.9 % was found and taken into account as a corrective factor in the collected charge. All the measurements were repeated. A further verification was carried out for ^{209}Bi. A thinner target (1.04 mg/cm^2 thick) was run at 30°, 60°, 90° and 120°. The situation for this target was similar to the other elements. Good agreements were obtained for the measurements corresponding to both thicknesses.

Due to the non-uniformity of the ^{59}Co target and to the charge collection problem with ^{209}Bi, the runs were taken for fixed target normal-beam direction angles, which took advantage of the good resolution of the detectors, because there were no possibilities of elastic and inelastic peaks superposition, since the first excited levels for ^{59}Co and ^{209}Bi are at 1.097 and 0.894 MeV, respectively. The $+20°$ and $-20°$ angles for the first and second quadrant for ^{59}Co and $+10°$, $-10°$ for ^{209}Bi were taken, respectively.

In this way practically the same target area was exposed to the beam in the whole angular distribution. At the beginning, a monitor was used at a fixed position near 24° to check the reproducibility of the positions of the targets, since the target holder assembly was freely retractable for their protection [23]) during scattering chamber operations.

The target thicknesses were measured by the gravimetric technique. A microbalance of 10 μg precision and a microscope for measuring the areas were used.

The ^{59}Co target was made by electrolytic deposition, and its thickness was 2.47 mg/cm^2.

The ^{209}Bi targets were obtained by the evaporation method using a formvar backing. Target thicknesses of 2.99 and 1.04 mg/cm^2 were obtained.

The thickness uniformity of the targets was investigated by using a collimated ^{241}Am alpha source and an energy calibrated multi-channel analyser. By interposing the targets as absorbers, it was possible to find their uniformity, being better than 1 % for ^{209}Bi. For ^{59}Co, on the contrary, a lack of uniformity of 8.1 % was found. To

investigate if the average thickness obtained via the gravimetric technique had a meaning at all, the thickness inside the beam spot was calculated by using the relative mass stopping power S_m [see ref. [30])]. A target of ^{48}Ti available for other studies [31]) was chosen among others as element of reference due to its good uniformity and the good precision with which its thickness was known. Its thickness and higher Z also produced a larger α-peak displacement in the multi-channel analyser, improving the precision of the method, and their similar atomic numbers compensate some effects on the relative mass stopping powers.

The average ionization potential has been calculated with the Bloch formula $I = kZ$, k being extracted from the Bichsel values [32]). The measurements were taken for target-in and target-out positions. Both elements were investigated in three different places inside the beam spot. In the first position the peak was at channel 351. In the second one it was at channels 228.0-228.5 and 228.0 for ^{48}Ti and at channels 276.5-279.0 and 273.0 for ^{59}Co. A difference less than 2.5 % of the calculated thickness was obtained when compared with the gravimetric value. The sensitivity of the method permitted determination of thickness variations of the order of 15 μg/cm^2.

Taking into consideration the vernier precision for measuring angles [23]) and the optical and kinematic tests of alignment, the errors for the target and observation angles were estimated to be less than $\pm 0.2°$.

Special precautions were taken to control the collected charge measurements, and repeated calibrations of the integrator were carried out. The error may be estimated within 1 %.

The statistical errors were kept less than 1 % in most cases, unless small cross sections forced a larger error.

The estimated deadtime errors were zero. An additional check was provided by a comparison between the measured and the Rutherford cross sections at small angles, when a much higher counting rate was available and the elastic process was almost pure Coulomb scattering. A significant agreement was obtained.

The background errors were estimated by taking extreme background subtraction curves, averaging and taking as error the deviation from the average value. Due to the elastic and inelastic peaks separation and the small, low-energy tail of the detectors, these errors were usually smaller than 0.5 %.

Geometrical errors, including the solid-angle error due to the cover plate deflection [23]), were kept smaller than 0.1 %.

The errors corresponding to the targets thicknesses were around 2 %.

The last two errors affect the absolute values of the cross sections but not the relative ones, since they are systematic errors. The optical-model calculations are sensitive to the shape of the angular distributions.

3. Results and discussion

The isospin term in the nuclear optical potential was studied on ^{59}Co and ^{209}Bi. The elements were selected because they are 100 % pure, and thus spurious effects due

to isotopic admixtures are avoided. Also, complete neutron angular distributions were available for them in tables with numerical values and quoted errors for the differential cross sections, and their total and non-elastic cross sections for neutrons have been measured by different groups with good accuracy.

The proton energy was $E_p = 14.4 \pm 0.1$ MeV.

Besides the favourable fact that a large amount of neutron data is available at 14 MeV energy, and additional advantage for optical-model proton elastic scattering studies relies on the fact that there is practically no proton contamination due to compound elastic scattering ($\sigma_{C.E.} = 0$), since at this energy we are several MeV above the (p, n) threshold for these nuclei, which constitutes a preferential channel for compound nucleus de-excitation [34-36]).

The following expression gives the potential that has been taken:

$$V = V_c(r) - V_S f_S(r) - iW_D f_D(r) - V_{s.o.} \left(\frac{\hbar}{m_\pi c}\right)^2 \left[-\frac{1}{r}\frac{df_S}{dr}\right] \sigma \cdot l, \tag{3}$$

where

$$f_S(r) = \left[1+\exp\left(r-\frac{R_S}{a_S}\right)\right]^{-1}, \qquad R_S = r_S A^{\frac{1}{3}},$$

$$f_D(r) = 4\exp\left(r-\frac{R_D}{a_D}\right) \Big/ \left[1+\exp\left(r-\frac{R_D}{a_D}\right)\right]^2, \qquad R_D = r_D A^{\frac{1}{3}},$$

$$V_c(r) = Z_I Z_T e^2/r, \qquad r \geqq R_S,$$

$$= Z_I Z_T e^2 \left(3-\frac{r^2}{R_S^2}\right) \Big/ 2R_S, \qquad r < R_S.$$

The Coulomb radius has been taken equal to R_S since results are not sensitive to it. Here Z_I and Z_T denote the incident particle and target atomic numbers, respectively, while V_S, W_D and $V_{s.o.}$ are the potential depths (positive numbers).

From eqs. (1) and (2),

$$C = \frac{\Delta V}{2\dfrac{N-Z}{A}}.$$

The correction V_c due to the energy dependence of V is included in ΔV.

After several trials to fit the available data, it was found that the best parameters were those due to Perey [21]), which were obtained from an extension analysis of data for a wide range of nuclei and for energies between 9 and 22 MeV. Therefore we used

$$r_S = 1.25 \text{ fm}, \qquad a_S = 0.65 \text{ fm},$$
$$r_D = 1.25 \text{ fm}, \qquad a_D = 0.47 \text{ fm}.$$

An intermediate value of $V_{s.o.} = 8$ MeV was used.

The analysis was made with a computer by using an automatic parameter search code in conjunction with the optical-model code.

The fits were judged quantitatively according to the quantity χ^2, defined as

$$\chi^2 = \frac{1}{N}\sum_{i=1}^{N}\left[\frac{\sigma_T(\theta_i)-\sigma_E(\theta_i)}{\Delta\sigma_E(\theta_i)}\right]^2.$$

Here, $\sigma_T(\theta_i)$ and $\sigma_E(\theta_i)$ denote the calculated and experimental cross sections at θ_i, respectively, and $\Delta\sigma_E(\theta_i)$ the corresponding experimental error.

When V and W_D were varied simultaneously, the final values for W_D differ from the known trends [21]) for A and Z for protons. Finally W_D was fixed and V varied. An intermediate value $W_D = 10$ MeV was finally taken.

It is sometimes found that by calculating $\sigma_T - \sigma_E$ for each point, these differences are predominantly of one sign and indicate a difference in the absolute normalization between the two curves. This may be remedied by introducing a normalization factor λ that takes this fact into account [37]).

TABLE 1

Best fit parameters for elastic proton scattering from ^{59}Co

No.	V_S (MeV)	W_D (MeV)	$V_{s.o.}$ (MeV)	V_c (MeV)	σ_A (mb)	λ	χ^2
1	49.32	10.0	8.0	2.774	949	1.0	69.1
2	49.391	10.0	8.0	2.774	949	1.082	52.2
3	48.987	13.70	7.5	2.774	995	1.0	11.7

3.1. STUDY ON $^{59}_{27}Co_{32}$

The results for protons are summarized in table 1. In No. 3 the imaginary optical potential W_D was taken equal to the more plausible value for protons determined from the formula obtained by Perey over a range of nuclei [21])

$$W_D = 9.8 + 46\,\frac{N-Z}{A} = 13.70 \text{ MeV}.$$

Since W_D was taken fixed, the same value was adopted for neutrons. For the spin-orbit potential, $V_{s.o.} = 7.5$ MeV.

The fits obtained for No. 1, 2 and 3 of table 1 are illustrated in figs. 2-4, respectively. As can be observed in fig. 3, the fit is improved with respect to that of fig. 2 in the region 30°-50° and for angles larger than 90° due to the normalization. From fig. 4 it can be seen that there is a much better agreement at the first minimum near 70° and for backward angles.

The corresponding results for neutrons are summarized in table 2.

The neutron elastic scattering data from ^{59}Co have been extracted from the results obtained by St. Pierre *et al.* [38]), published as tables, with numerical values and

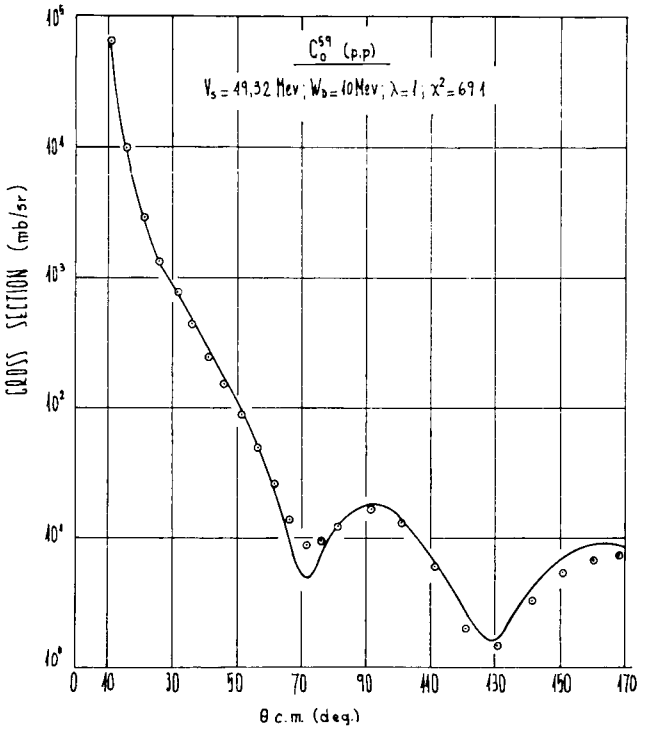

Fig. 2. Proton elastic angular distribution corresponding to ^{59}Co and theoretical optical-model fit (table 1, No. 1).

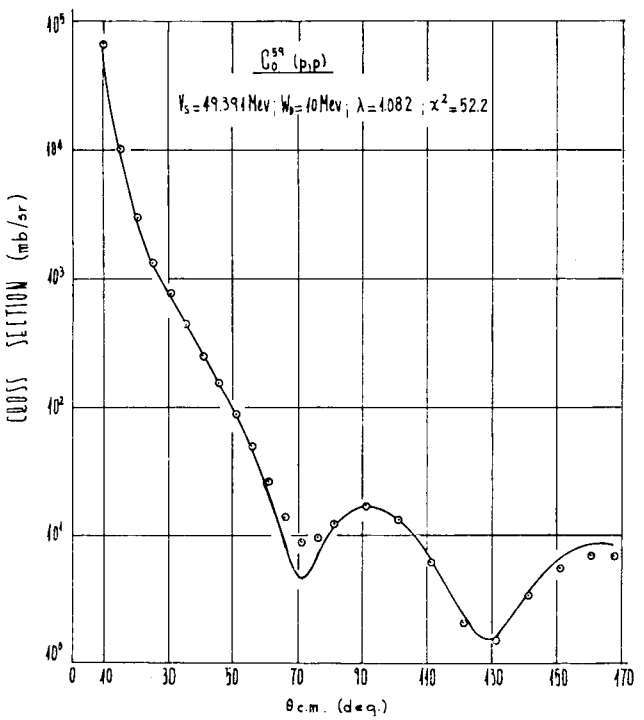

Fig. 3. Elastic proton scattering on ^{59}Co (table 1, No. 2).

quoted errors for the differential cross sections by Howerton [39]). The neutron energy was $E_n = 14.3 \pm 0.3$ MeV.

The experimental total (σ_T) and non-elastic (σ_n) cross sections are

$$\sigma_T = 2.72 \pm 0.05\text{b, ref.}^{40}),$$
$$\sigma_n = 1.37 \pm 0.03\text{b, ref.}^{41}).$$

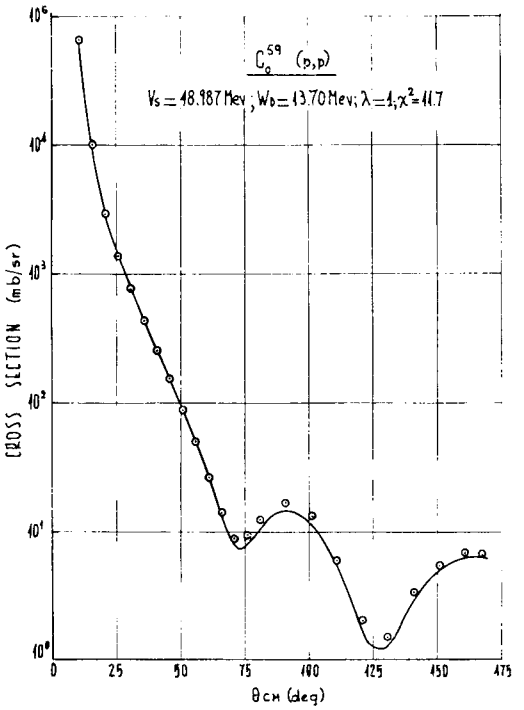

Fig. 4. Optical-model fit for ^{59}Co (p, p), with the new parameters $W_D = 13.70$ MeV; $V_{s.o.} = 7.5$ MeV (table 1, No. 3).

TABLE 2

Best fit parameters for elastic neutron scattering from ^{59}Co

No.	V_S (MeV)	W_D (MeV)	$V_{s.o.}$ (MeV)	σ_T (b)	σ_A (b)	λ	χ^2
4	42.13	10.0	8.0	2.51	1.40	0.824	12.2
5	42.382	13.70	7.5	2.61	1.50	1.0	35.8

The fits obtained for Nos. 4 and 5 of table 2 are shown in figs. 5 and 6, respectively. From χ^2 and fig. 6, it can be seen that for the last case the fit is worse. This result, however, is partly due to the fact that no normalization has been used.

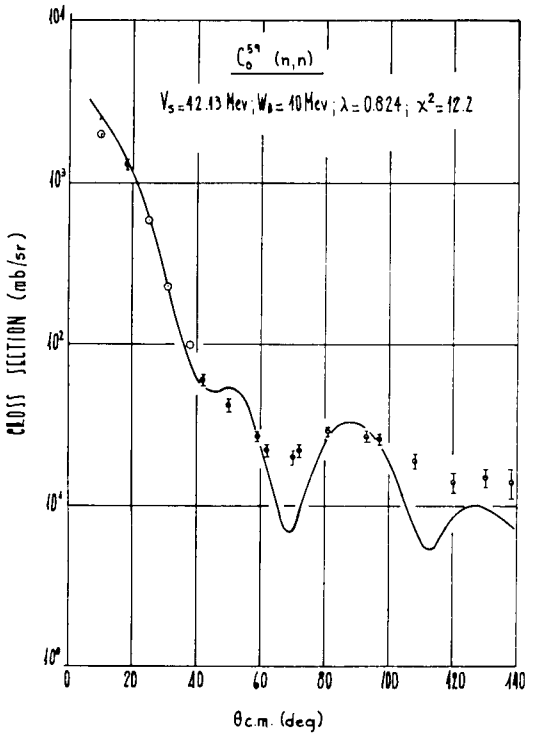

Fig. 5. Elastic neutron scattering on ^{59}Co, data from refs. [38,39]) (table 2, No. 4).

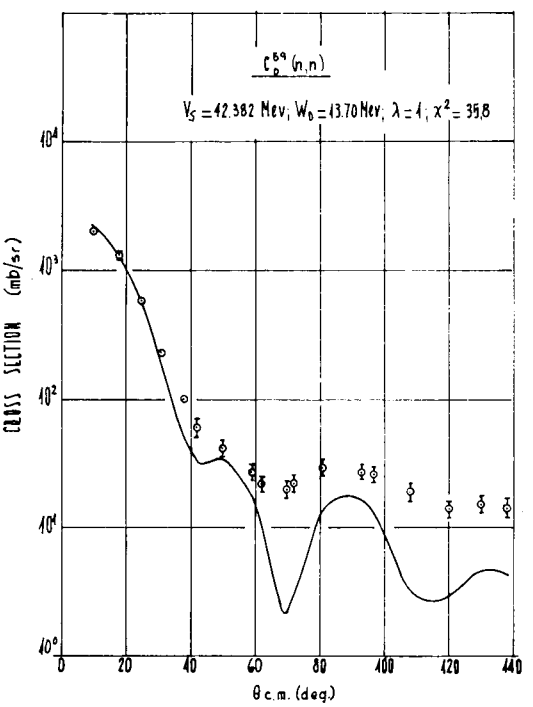

Fig. 6. Optical-model fit for ^{59}Co(n, n), with the new parameters; $W_D = 13.70$ MeV; $V_{s.o.} = 7.5$ MeV (table 2, No. 5).

Combining 1 and 4 it is obtained: $C = 26.1$ MeV.

Combining 2 and 4 it is obtained: $C = 26.5$ MeV.

Combining 3 and 5 it is obtained: $C = 22.6$ MeV.

The second result shows that the situation is not critical with regard to the new fitting, obtained by normalization.

TABLE 3

Best fit parameters for elastic proton scattering from ^{209}Bi

No.	V_S (MeV)	W_D (MeV)	$V_{s.o.}$ (MeV)	V_c (MeV)	σ_A (mb)	λ	χ^2
1	56.74	10.0	8.0	5.594	643	1.0	5.2
2	57.153	19.26	7.5	5.594	668	1.0	29.3

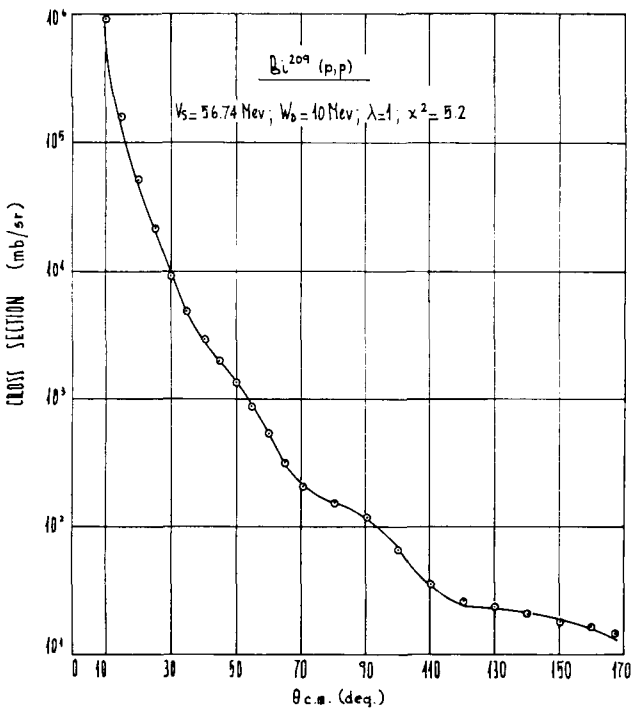

Fig. 7. Proton elastic scattering on ^{209}Bi and optical-model theoretical curve (table 3, No. 1).

3.2. STUDY ON $^{209}_{83}Bi_{126}$

The results obtained for protons are summarized in table 3. In No. 2 the imaginary optical potential was fixed according to the above mentioned trend for protons. The corresponding fits are shown in figs. 7 and 8, respectively.

The elastic neutron scattering data were extracted from the study of Rayburn [42]) at an energy of E_n = 14 MeV in the angular range 10°-165°, and from another study due to Yuasa [43]) at E_n = 14.1 ± 0.2 MeV in the range 70°-170°. In both cases the tabulated values are found in ref. [39]).

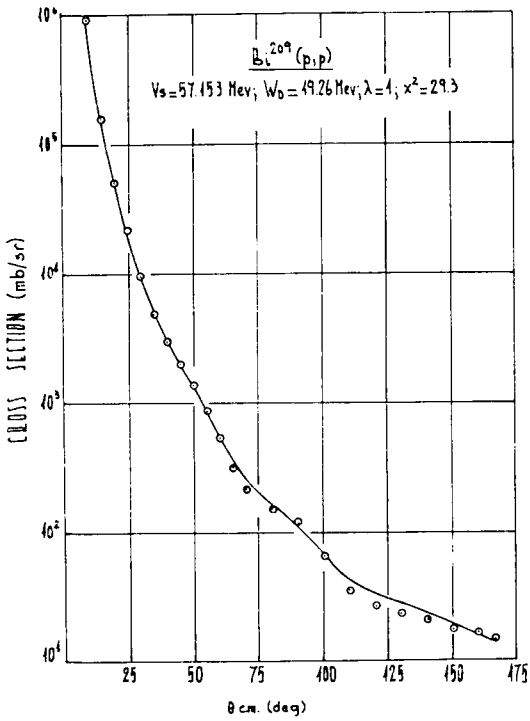

Fig. 8. Proton elastic scattering on ^{209}Bi and theoretical curve corresponding to parameters given in table 3, No. 2.

TABLE 4
Best fit parameters for elastic neutron scattering from ^{209}Bi

No.	V_S (MeV)	W_D (MeV)	$V_{s.o.}$ (MeV)	σ_T (b)	σ_A (b)	λ	χ^2
3	41.83	10.0	8.0	5.36	2.53	1.0	7.1
4	42.58	10.0	8.0	5.28	2.53	0.824	5.4
5	41.626	19.26	7.5	5.42	2.85	1.0	18.4

The experimental total and non-elastic cross sections are

σ_T = 5.17 ± 0.17, ref.[44]), σ_n = 2.56 ± 0.05, ref.[46]),
= 2.53 ± 0.02, ref.[47]),
= 5.46 ± 0.11, ref.[40]) = 2.50 ± 0.07, ref.[48]),
= 2.56 + 0.04, ref.[41]),
= 5.44 ± 0.05, ref.[45]) = 2.59 ± 0.03, ref.[49]).

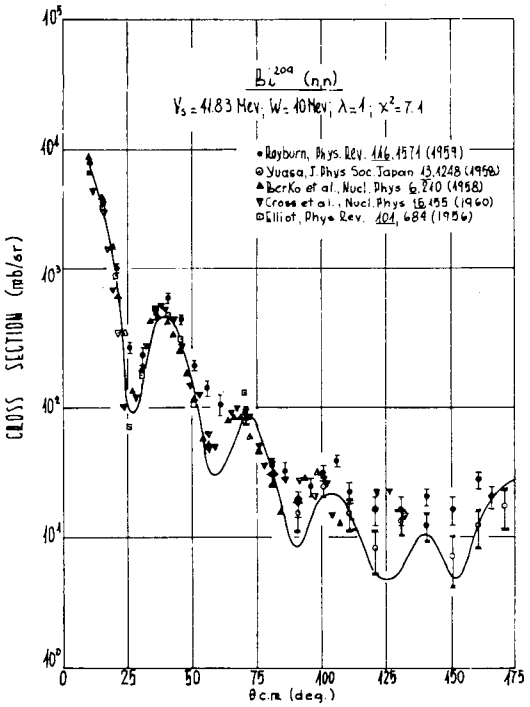

Fig. 9. Neutron elastic scattering on ^{209}Bi and optical-model theoretical curves. Symbols are: ● ref. [42]), ○ ref. [43]), △ ref. [52]), ▽ ref. [51]) and □ ref. [50]) (table 4, No. 3).

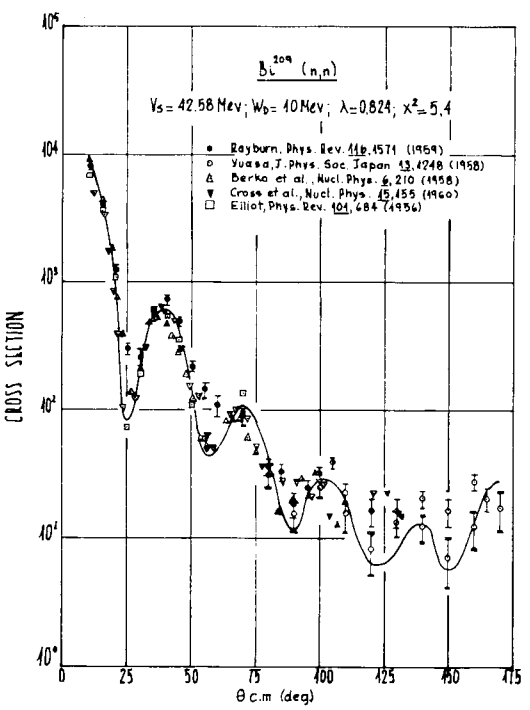

Fig. 10. Neutron elastic scattering on ^{209}Bi and normalized ($\lambda = 0.824$) optical-model theoretical curve. See caption to fig. 9 (table 4, No. 4).

Values of refs. [40,44]) were taken at E_n = 14 MeV; that of ref. [45]) at E_n = 14.37 MeV. The non-elastic results were determined at an energy E_n approximately equal to 14.1 MeV.

The corresponding results for neutrons are summarized in table 4.

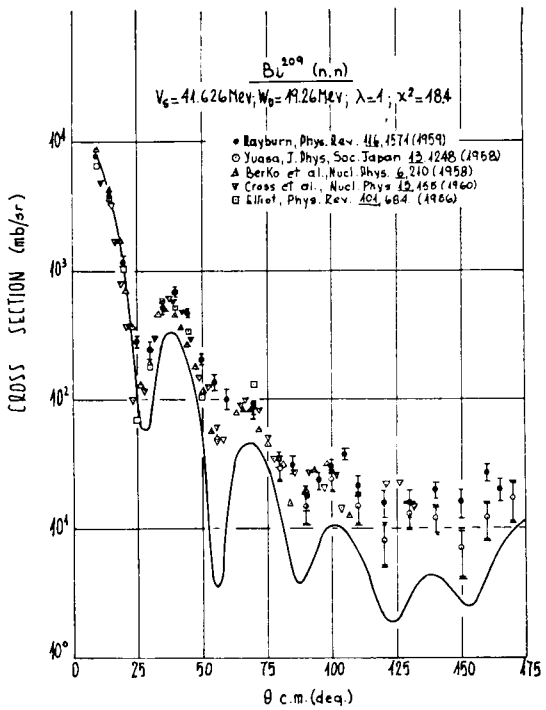

Fig. 11. Neutron elastic scattering on ^{209}Bi and theoretical curve for parameters of No. 5, table 4.

TABLE 5

Best fit parameters when V_S and W_D are allowed to vary

Reaction	V_S (start) (MeV)	W_D(start) (MeV)	V_S (MeV)	W_D (MeV)	σ_T (b)	σ_A (b)	χ^2
^{59}Co(p, p)	55	12	48.997	13.637		0.995	11.6
^{59}Co(n, n)	45	12	43.419	7.175	2.50	1.26	7.5
^{209}Bi(p, p)	55	18	56.715	11.259		0.654	4.2
^{209}Bi(n, n)	45	18	41.207	7.482	5.47	2.29	4.1

In fig. 9 is shown the fit obtained with the Rayburn data [42]) (full circles) and with those of Yuasa [43]) (open circles) for which tabulated values were available [39]), and corresponds to No. 3 of table 4. The data independently obtained by Elliot [50]), by Cross and Jarvis [51]) and by Berko *et al.* [52]) have been plotted for illustrative

purposes, although no numerical values were available. Those values have been read out directly from enlarged figures. It is to be noted that the theoretical curve has too deep minima when compared with the data used for the calculations, although there is a good agreement with the other published results.

Figs. 10 and 11 show the fits corresponding to Nos. 4 and 5 of table 4. In the latter case the fit, without normalization, is much worse than in the previous cases.

On the other hand, the agreements between experimental and theoretical total and non-elastic cross sections a.e very good for cases 3 and 4.

Combining 1 and 3 it is obtained: $C = 22.6$ MeV.
Combining 1 and 4 it is obtained: $C = 20.8$ MeV.
Combining 2 and 5 it is obtained: $C = 24.1$ MeV.

From an analysis of the results when the imaginary optical potentials W_D are increased, it is observed that the fits for neutrons are in those cases much worse. If, consequently, one allows the simultaneous variation of V_S and W_D, but starting from initial values near the expected ones, according to systematics, to avoid a spurious minimum in parameter multispace, one obtains the results shown in table 5; $V_{s.o.}$ was equal to 7.5 MeV.

However, starting from different values ($V_S = 40$ MeV and $W_D = 10$ MeV for both, protons and neutrons) quite similar results were obtained. The only exception was ^{209}Bi(p, p). In that case χ^2 was equal to 24.0, against 4.2 as shown in the table.

With the results summarized in the preceding table, we find

for the nucleus ^{59}Co: $C = 16.5$ MeV, and
for the nucleus ^{209}Bi: $C = 24.1$ MeV.

The corresponding fittings can be observed in figs. 12–15, respectively.

For the reaction ^{209}Bi(n, n) only the points that were used for the calculations have been plotted in fig. 15, in order to make easier the judgement of the fitting. Here the absorption cross sections are a little smaller, and the total cross sections are almost the same.

From the analysed results it is possible to see that increasing W_D for neutrons, the fits grow worse. This is confirmed by the results shown in table 5, where the W_D values for neutrons are smaller than for protons. This may be indicative of a symmetry term for the imaginary part of the potential, as found by Satchler [53]). From the stated figures, however, the coefficient for the term $\pm(N-Z)/A$ is quite different if calculated from ^{59}Co or ^{209}Bi, the constant term being around 10 MeV.

On the other hand, it should be noted that, for protons, W_D for ^{59}Co is larger than for ^{209}Bi. This, as stated at the beginning of this analysis, is against the known [21]) trend for W_D.

According to the simultaneous optical analysis of results for both types of nucleons, when the imaginary optical potential is kept fixed, it is found that the coeffi-

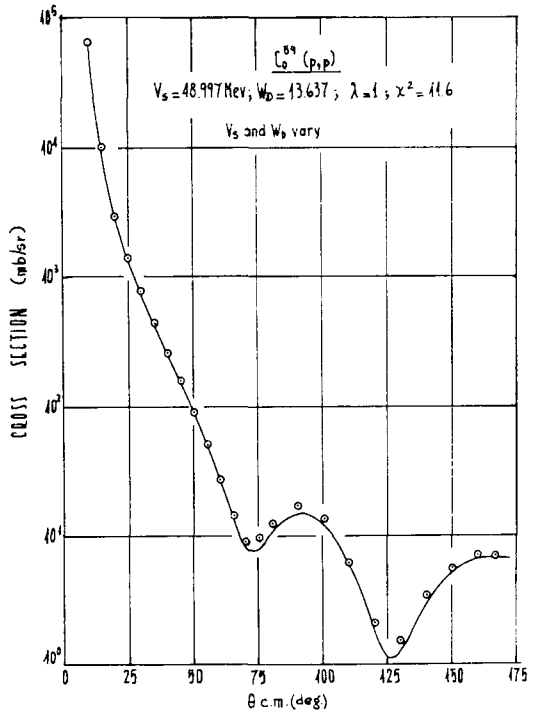

Fig. 12. The ^{59}Co(p, p) reaction and fitting obtained by varying V_S and W_D.

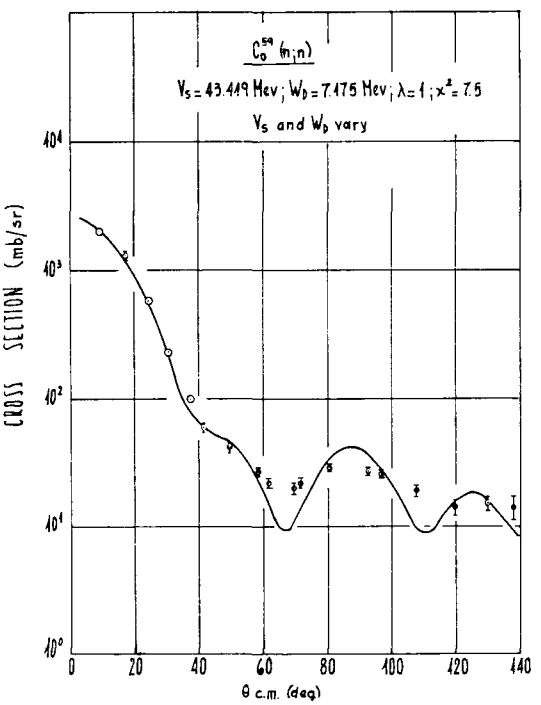

Fig. 13. The ^{59}Co(n, n) reaction and fitting obtained by varying V_S and W_D.

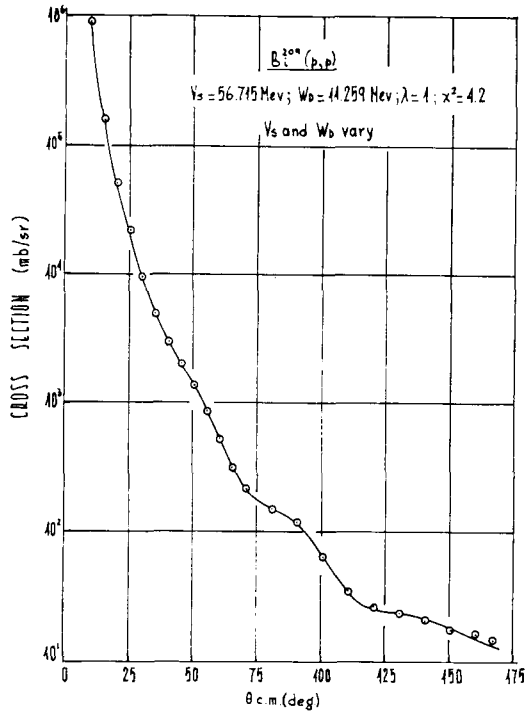

Fig. 14. The ^{209}Bi(p, p) reaction and fitting obtained by varying V_S and W_D.

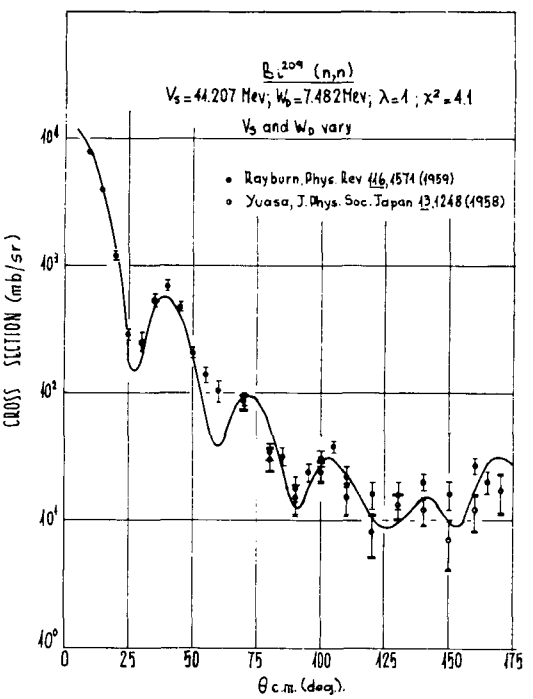

Fig. 15. The ^{209}Bi(n, n) reaction and fitting obtained by varying V_S and W_D.

cient of the nuclear symmetry parameter would be around

$$C = 23.8 \pm 3 \text{ MeV}.$$

When only results corresponding to best fits are taken into consideration, those for varying V_S and W_D included, it is obtained

$$C = 22.8 \pm 4 \text{ MeV}.$$

(Results for $W_D = 13.70$ MeV and 19.26 MeV are excluded.)

It is worthwhile to emphasize that with the C value determined in this study it has been possible to obtain the best V_S value for a good fitting for the nucleus ^{46}Ti, starting from a previous fit for ^{48}Ti in a study carried out on these nuclei [31]).

The ^{27}Al nucleus was also chosen for the study. With this element, however, it was not possible to get a good fit for reasonable parameters of the optical model. This may be due to collective effects that invalidate the model [54]). Moreover, as the neutron excess is very small for this nucleus ($N-Z = 1$) any uncertainty in the values of the potentials, has a large effect on the C constant. Therefore, this constant was larger by a factor around 2 with regard to the predetermined values.

Hodgson [22]) analysed all the available data obtained via different classes of studies. The coefficient of the nuclear symmetry parameter ranged from 16.3 to 50 MeV. Perey [21]) estimated this coefficient to be of the order of 30 ± 10 MeV.

More recently Hodgson [55]) estimated the best value to be around 24 ± 4 MeV.

The results obtained in this study show good agreement with the figure stated above.

I would like to thank Dr. P. E. Hodgson for suggesting this work, the late Dr. Charles Gallagher, Jr., for his help in an early stage of preparation of the experimental set-up, the Pupin cyclotron crew for their able operation of the machine, Columbia University for allowing me the use of its facilities, the International Atomic Energy Agency and the US National Academy of Sciences for the award of a fellowship that made this work possible.

References

1) M. H. Johnson and E. Teller, Phys. Rev. **98** (1955) 783
2) A. E. S. Green and K. Lee, Phys. Rev. **99** (1955) 772
3) A. E. S. Green, Phys. Rev. **99** (1955) 1410
4) M. A. Melkanoff, S. A. Moszkowski, J. Nodvik and D. S. Saxon, Phys. Rev. **101** (1956) 507
5) L. Wilets, Phys. Rev. **101** (1956) 1805
6) A. E. S. Green, Phys. Rev. **102** (1956) 1325
7) A. A. Ross, H. Mark and R. D. Lawson, Phys. Rev. **102** (1956) 1613
8) A. A. Ross, R. D. Lawson and H. Mark, Phys. Rev. **104** (1956) 401
9) A. E. S. Green, Phys. Rev. **104** (1956) 1617
10) H. A. Bethe, Physica **22** (1956) 941
11) A. E. S. Green, K. Lee and R. J. Berkley, Phys. Rev. **104** (1956) 1625
12) A. M. Lane, Revs. Mod. Phys. **29** (1957) 193
13) M. A. Melkanoff, J. Nodvik and D. S. Saxon, Phys. Rev. **106** (1957) 793

14) S. Rand, Phys. Rev. **107** (1957) 208
15) A. E. S. Green and P. C. Sood, Phys. Rev. **111** (1958) 1147
16) L. A. Sliv and V. A. Volchok, JETP (Sov. Phys.) **36** (1959) 374
17) G. R. Satchler, Phys. Rev. **109** (1958) 429
18) A. M. Lane, Compt. Rend. Congr. Int. Phys. Nucl., Paris, juillet, 1958 (Dunod Cie., Paris, 1959) pp. 32-34
19) A. M. Lane, Phys. Rev. Lett. **8** (1962) 171
20) A. M. Lane, Nuclear Physics **35** (1962) 676
21) F. G. Perey, Phys. Rev. **131** (1963) 745
22) P. E. Hodgson, Phys. Lett. **3** (1963) 352
23) H. J. Erramuspe and A. Seifert, Nucl. Instr. **40** (1966) 155
24) W. Hansen and F. S. Goulding, Nat. Acad. Sci., Publ. 871 (1961)
25) J. Benveniste, R. Booth and A. Mitchell, UCRL-7427
26) G. Amsel and O. Smulkowski, IRE Trans. Nucl. Sci., N.S. **8** (1960) 21
27) S. Kobayashi, J. Phys. Soc. Japan **15** (1960) 1164;
Y. Nagahara, J. Phys. Soc. Japan **16** (1961) 133
28) J. Hahn and R. Mayer, Columbia University Report, unpublished
29) A. B. Gillespie, Signal, noise and resolution in nuclear counter amplifiers (Pergamon, London, 1953)
30) R. D. Evans, The Atomic nucleus (McGraw-Hill, New York, 1955)
31) H. J. Erramuspe, to be published
32) H. Bichsel, R. F. Mozley and W. A. Aron, Phys. Rev. **105** (1957) 1788;
H. Bichsel, Phys. Rev. **112** (1958) 1089
33) J. Benveniste, A. C. Mitchell and C. B. Fulmer, Phys. Rev. **129** (1963) 2173
34) L. I. Bolotin, A. P. Klyucharev, E. I. Revutzkii and N. I. Rutkevich, Proc. Int. Conf. Nucl. Structure, Kingston, (Univ. of Toronto Press, 1960) p. 169
35) R. A. Vanetsian, G. F. Timoshevskii and E. D. Fedchenko, JETP (Sov. Phys.) **13** (1961) 842
36) V. Ya. Golovnya, A. P. Klyncharev and B. A. Shilyaev, JETP (Sov. Phys.) **14** (1962) 25
37) P. E. Hodgson, The optical model of elastic scattering (Oxford, 1963)
38) C. St. Pierre, M. K. Machive and P. Lorrain, Phys. Rev. **115** (1959) 999
39) R. J. Howerton, UCRL-5573 (1961)
40) J. H. Coon, E. R. Graves and H. H. Barschall, Phys. Rev. **88** (1952) 562
41) M. H. MacGregor, W. P. Ball and R. Booth, Phys. Rev. **108** (1957) 726
42) L. A. Rayburn, Phys. Rev. **116** (1959) 1571
43) K. Yuasa, J. Phys. Soc. Japan **13** (1958) 1248
44) E. Amaldi, D. Bocciarelli, B. N. Cacciapuoti and G. C. Trabacchi, Nuovo Cim. **3** (1946) 15
45) A. Bratenahl, J. M. Peterson and J. P. Stoering, Phys. Rev. **110** (1958) 927
46) D. D. Phillips, R. W. Davis and E. R. Graves, Phys. Rev. **88** (1952) 600
47) E. R. Graves and R. W. Davis, Phys. Rev. **97** (1955) 1205
48) H. L. Taylor, O. Lönsjö and T. W. Bonner, Phys. Rev. **100** (1955) 174
49) N. N. Flerov and V. M. Talyzin, J. Nucl. Energ. **4** (1957) 529
50) J. O. Elliot, Phys. Rev. **101** (1956) 684
51) W. G. Cross and R. G. Jarvis, Nuclear Physics **15** (1960) 155
52) S. Berko, W. D. Whitehead and B. C. Groseclose, Nuclear Physics **6** (1958) 210
53) G. R. Satchler, to be published
54) H. Niewodniczański, J. Nurzyński and A. Strzałkowski, J. Phys. Rad. **24** (1963) 944;
H. Niewodniczański *et al.*, Nuclear Physics **55** (1964) 386
55) P. E. Hodgson, Compt. Rend. Congr. Intern. Phys. Nucl. Paris, (1964) Vol. 1, p. 257

PRINTED IN THE NETHERLANDS